JACS
JOURNAL OF THE AMERICAN CHEMICAL SOCIETY

Article

pubs.acs.org/JACS

Integrating DNA-Strand-Displacement Circuitry with Self-Assembly of Spherical Nucleic Acids

Dongbao Yao,[†] Tingjie Song,[†] Xianbao Sun,[†] Shiyan Xiao,*[,†] Fujian Huang,[†] and Haojun Liang*[,†,‡]

[†]CAS Key Laboratory of Soft Matter Chemistry, iChEM (Collaborative Innovation Center of Chemistry for Energy Materials), Department of Polymer Science and Engineering, and [‡]Hefei National Laboratory for Physical Sciences at the Microscale, National Synchrotron Radiation Laboratory, University of Science and Technology of China, Hefei, Anhui 230026, P. R. China

Supporting Information

ABSTRACT: Programmable and algorithmic behaviors of DNA molecules allow one to control the structures of DNA-assembled materials with nanometer precision and to construct complex networks with digital and analog behaviors. Here we developed a way of integrating a DNA-strand-displacement circuit with self-assembly of spherical nucleic acids, wherein a single DNA strand was used to initiate and catalyze the operation of upstream circuits to release a single strand that subsequently triggers self-assembly of spherical nucleic acids in downstream circuits, realizing a programmable kinetic control of self-assembly of spherical nucleic acids. Through utilizing this method, single-nucleotide polymorphisms or indels occurring at different positions of a sequence of oligonucleotide were unambiguously discriminated. We provide here a sophisticated way of combining the DNA-strand-displacement-based characteristic of DNA with the distinct assembly properties of inorganic nanoparticles, which may find broad potential applications in the fabrication of a wide range of complex multicomponent devices and architectures.

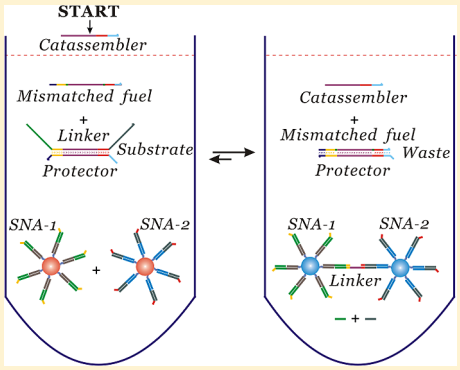

INTRODUCTION

In the field of dynamic DNA nanotechnology, a reaction known as toehold-mediated DNA-strand displacement,[1] wherein a single-stranded sequence of contiguous bases (called toehold) that facilitates the branch migration processes on a duplex helix are adopted to displace the sequestered single strand, has demonstrated its capability to build complex autonomous systems.[2,3] The emergence of the new methodology has enabled the creation of sophisticated ways of constructing diverse molecular dynamic systems, including programmed self-assembly of nanostructures, to form a variety of DNA patterns,[4,5] molecular gears constructed by DNA nanocircles,[6] autonomous DNA walkers that move along a self-assembled track,[7−9] cascading nanomachines that could achieve powerful signal amplification of input signals,[10,11] molecular robots guided by prescriptive landscapes,[12] and synthetic molecular motors capable of autonomous nanoscale transport.[13] In particular, toehold-mediated DNA-strand displacement has been ingeniously implemented in entropy-driven and enthalpy-driven catalytic reaction construction,[14,15] DNA catalyst network guided DNA tile self-assembly,[16] synthetic transcriptional clocks,[17] and digital circuit computation.[18−20] In these systems, oligonucleotide strands act as catalysts or inputs that fuel the DNA-based molecular machine through a series of toehold strand-displacement reactions in a "geometry-free-like" network.

On the other hand, polyvalent nucleic acid−nanoparticle conjugate, an inorganic nanoparticle functionalized with nucleic acids on the surface, was synthesized using a gold core and oligonucleotide shell in the mid-1990s,[21,22] and it represents the first well-characterized form of spherical nucleic acid (SNA) conjugates.[23] This unique structure possesses the hybridized properties of both inorganic gold nanoparticles (AuNPs) and organic nucleic acid strands. The gold core, except as a scaffold for assembling and orienting the nucleic acid strands into a dense arrangement, contributes to the conjugate specific physical and chemical properties, such as plasmonic,[24,25] catalytic,[26] scattering,[27] and quenching,[28] whereas the outside nucleic acid shell endows conjugates with stability in solution, due to its hydrophilic character, and serves simultaneously as a reaction group for mediating the reactivity of the conjugates. In addition, such an established approach allows the synthesis of SNA conjugates into a broad variety of microstructures, from a disordered−amorphous morphology to periodic lattice crystal-like structures.[29,30] These materials have now catalyzed worldwide interest in using such well-characterized nanostructures as novel labels for in vitro assays[31] and intracellular detection,[32] and as powerful cell transfection,[33,34] gene regulation,[35] therapeutics,[36] biodiagnostics,[37] medicine,[38] biosensors in terms of colorimetric-based assays,[39−42] programmed nanostructures assembly,[43−46] electronic-based detection,[47] and Raman-based detection.[48]

Received: July 16, 2015
Published: October 20, 2015

DOI: 10.1021/jacs.5b07453
J. Am. Chem. Soc. 2015, 137, 14107−14113

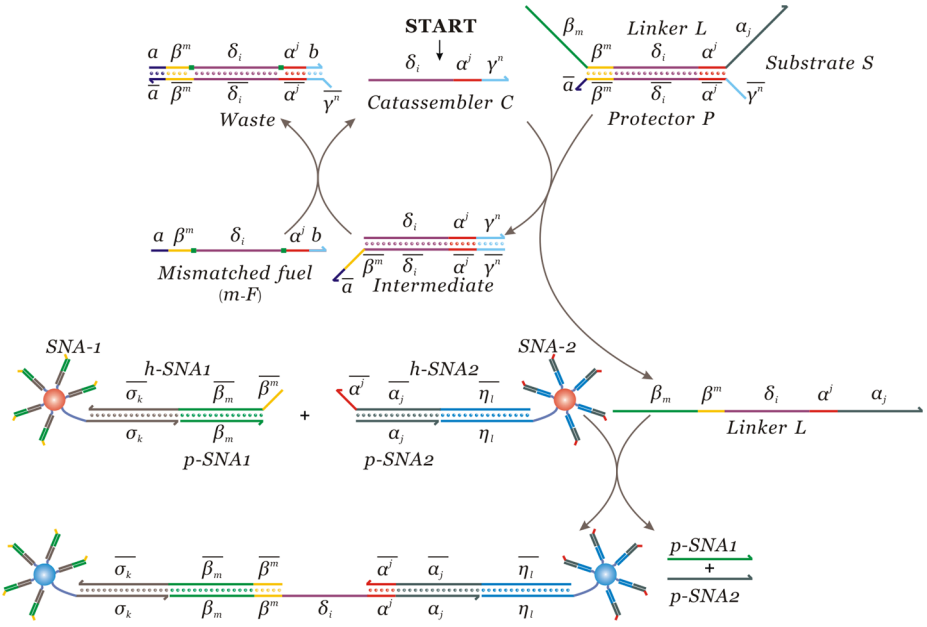

Figure 1. Graphical representation of the integrating catalytic circuit with self-assembly of SNA conjugates.

In some of these applications, assembly of SNA conjugates is required in order to achieve the desired functions. Traditionally, the direct-linker-addition approach is employed, in which the assembly reactions are initiated by the addition of a target oligonucleotide molecule together with two types of SNAs to cause aggregations of SNA conjugates through hybridization with the probe molecules functionalized on SNA. However, bearing the multiple reactivity groups on the outside of the nucleic acid shell, SNA conjugate is supposed to be a versatile building block that allows the coupling of the programmability and algorithmic behavior of nucleic acids with the distinct assembly performance of SNA conjugates to achieve functions that are inaccessible in a simple system. In our earlier efforts,[49,50] a DNA nanomachine was devised and built to drive self-assembly of SNA conjugates. The nanomachine was essentially a catalytic strand-displacement circuit operating under a series of successive toehold-mediated strand-displacement reactions (TMSDRs). Although the established SNA assembly strategy was promising in fabricating hybridized nanomaterials, the significant sequence constraints imposed on the synthesis of SNA constituted a substantial challenge. As in the direct-linker-addition strategy, the assembly of SNA conjugates can only be triggered by specifically designed targets. Similarly, in the DNA-machine-driven strategy, the fuel strands that graft on SNA generally share a partial common sequence with the catalyst DNA strand. Therefore, a new type of SNA conjugate needs to be prepared each time to achieve compatibility with every new catalyst strand (usually a target DNA strand for detection). This process is clearly time-consuming and expensive.[51] Thus, the development of more sophisticated ways of attaining this goal is urgently needed in order to meet the large demand of diverse applications.

Herein, we report an integrated DNA-strand-displacement circuitry with self-assembly of spherical nucleic acids. In our proposed mechanism, the initiation of the cross-linking of SNA conjugates relies on the sequestered region of linker oligonucleotide, which is released through the upstream circuit built on the basis of toehold-mediated displacement reactions. Noticeably, the domains on the strands functionalized on the SNAs do not participate in reactions occurring in reaction systems. By combining these two circuitries, our design increases the space of potential trigger oligonucleotide sequences and enables the synthesized SNA conjugates to detect arbitrary trigger DNAs and output colorimetric signals. The systems underlying such a feature allow the same types of SNA to integrate with other catalytic DNA circuits, i.e., without repreparing new types of SNAs, which will circumvent the laborious processes usually required for the preparation of new types of SNAs. Moreover, the DNA circuitry and SNA assembly are two sequential steps, and these two steps can be optimized or regulated separately. This feature provides the possibility to regulate the assembly of SNA conjugates over a large rate span.

RESULTS AND DISCUSSION

Principle of Integrating Catalytic Circuit with Self-Assembly of SNA Conjugates. The strategy here for integrating a toehold-mediated strand-displacement catalytic circuit with a SNA assembly comprises two subsystems. The first one, shown in the upper panel of Figure 1, serves as the upstream circuit to release a single DNA strand, called linker L, that subsequently triggers the assembly of SNA conjugates in the second subsystem, shown in the lower panel of Figure 1. The single strand L plays the role of "connector" that bridges two subsystems. In Figure S1 of the Supporting Information (SI), we display the structures of the three molecules necessary for the construction of the system: first, a double-stranded DNA molecule, called substrate S, formed by L and another single strand called protector P (Figure S1a, SI); second, two types of double-stranded DNA molecules (Figure S1b, SI) composed of two pairs of single strands, (h-SNA1, p-SNA1) and (h-SNA2, p-SNA2); and, third, two sorts of SNA conjugates, called NP-1 and NP-2 (Figure S1c, SI). These SNA conjugates were further modified with the double-stranded DNA molecules prepared as outlined in Figure S1b (SI) for fabricating two new types of SNA conjugates, SNA-1 and SNA-2, the detailed processes of which are presented in Figure S1d (SI).

DOI: 10.1021/jacs.5b07453
J. Am. Chem. Soc. 2015, 137, 14107−14113

In the mixture of S, SNA-1, and SNA-2 (Figure 1), although two exposed domains, β_m and α_j, in L are able to trigger the SNA assembly through hybridizing the corresponding complementary domains, $\overline{\beta_m}$ and $\overline{\alpha_j}$, on SNA-1 and SNA-2, the latter two domains are initially protected by the single strands p-SNA1 and p-SNA2, respectively. As a result, instant cross-linking between SNA-1 and SNA-2 by L is effectively prohibited, yielding a stable system. However, once a small quantity of single DNA strand (called catassembler C in Figure 1) is introduced into the mixture, the self-assembly of SNA conjugates was immediately initiated and thereafter operated under the scenario of a series of TMSDRs. In a typical reaction cycle, shown in the upper panel of Figure 1 (details are given in Figure S2, SI), upon addition of C, the domain γ^n of C quickly binds onto its complement, $\overline{\gamma^n}$ (toehold), in P to initiate the first round of TMSDR, releasing L as well as generating a double-stranded intermediate composed of P and C. Then, the fuel strand m-F starts a new round of TMSDR with an intermediate molecule, yielding a double-stranded waste composed of P and m-F and releasing C that is reusable in the further reaction cycles.

Subsequently, the released L from the upstream circuit reacts with the DNA molecules on the surface of SNA conjugates in a new round of TMSDR, as shown in the lower panel of Figure 1 (the detailed procedure can be found in Figure S2, SI). The hybridization between the complementary domains on L and SNA-1 (or SNA-2), that is, domain β^m of L and domain $\overline{\beta^m}$ in h-SNA1 or (domain α^j of L and domain $\overline{\alpha^j}$ in h-SNA2), could result in the displacement of the prehybridized strands p-SNA1 and p-SNA2 and the cross-linking of SNAs.

Fuel Strand Design. In addition to the above-mentioned species, a fuel strand that is used to sustain the continuous running of the circuit constitutes another important component of the catalytic circuit.[18,52] We initially designed a fuel strand with domains β^m and α^j complementing perfectly with $\overline{\beta^m}$ in h-SNA1 and $\overline{\alpha^j}$ in h-SNA2, respectively. Unfortunately, rapid and unwanted SNA aggregations were observed (red line in Figure 2) when these two domains (β^m and α^j) are both five bases in length. We found that the aggregations could be effectively suppressed by cutting the domains into a short length of four bases. However, this presented us with another dilemma, because the shortened domain strand is not yet efficient when used as a fuel. To circumvent this difficulty, we adopted a mismatch-strand strategy.[53−55] According to the considerations of Turberfield and his co-workers,[55,56] toehold-mediated DNA displacement can be regulated over 3 orders of magnitude at a constant rate without significantly affecting free energy when introducing a mismatch along the strand in a position of the displacement domain near the invading toehold or at its end. Thus, in this strategy, we introduced two mismatched bases in domains β^m and α^j at the positions near the displacement domain. The details of the fuel-strand design are given in Figure S3 (SI). The sequences of domains β^m and α^j in strand fuel (Figure S3a, SI) were first mutated, respectively, by a single-base variation to generate strand fuel-1 (Figure S3b, SI), so that it becomes a four-base complementary sequence to the domains $\overline{\beta^m}$ or $\overline{\alpha^j}$ in P. Obviously, the strand tailored in such a manner cannot induce SNA aggregations, but it is not yet active as fuel. To restore its activity, we modified fuel-1 to yield the mismatched-fuel-strand, m-F (Figure S3c, SI), via prolonging the two ends of fuel-1 by a few bases (labeled as domain a and b in m-F in Figure S3c, SI) so that domain a is complementary with the dangling domain $\overline{\alpha}$ in P and domain b is partially complementary with domain $\overline{\gamma^n}$ of P. Such a modified fuel strand achieves an enhanced capability to displace C when reacting with the intermediate due to the lengthy toehold (Figure 1). Thus, we successfully devised the mismatched fuel strand, called m-F, which possesses two single-base mutations and three-base extensions at two ends of the original fuel strand [Figures 1 and S3 (SI)], whereby the system can sustain high stability in the absence of C, as illustrated by the black line in Figure 2, and gain high reactivity in the presence of C.

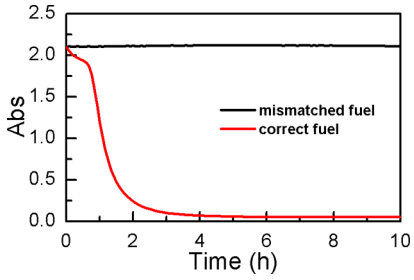

Figure 2. Difference in UV−vis absorbance between the correct fuel strand and the mismatched fuel strand on the influence of the SNA assembly. [fuel] = [m-F] = 3.92 μM, [SNA-1] = [SNA-2] = 4 nM.

Assessing SNA Assembly by Direct Addition of Linker Strand. Before investigating the integrated system, a second subsystem is first assessed via monitoring the kinetics of the assembly process of SNA conjugates when L is added directly. The experiment was performed by following time-resolved UV−vis absorption spectroscopy at 520 nm in varied concentrations of L. The kinetic profile with the feature of a gradual decay in absorbance (Figure 3) was qualitatively described with Avrami's law, Abs = Abs$_0$ exp{−[$(t - t_0)/\tau$]^n}, where the parameters n, t_0, and t are the Avrami exponent, reaction onset time, and reaction time, respectively, whereas the parameter τ is the characteristic time for describing the reaction rates of the SNA assembly. By fitting the kinetic plots in Figure 3a, we obtained the concentration dependence of τ shown in Figure 3b. The decrease in τ at high concentrations of linker L is indicative of an increased assembly rate. In particular, the remarkable decreases of τ values from 40.2 to 1.8 h on the scale from 39.2 to 137.4 nM implies the optimal concentrations for mediating the assembly rate.

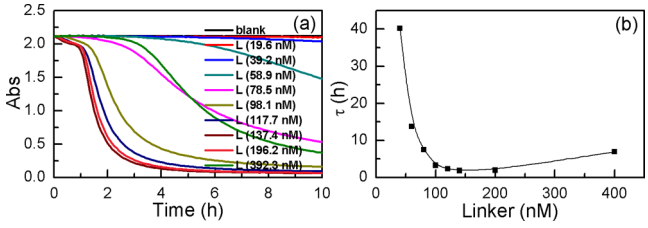

Figure 3. Assembly of SNA by the addition of linker strand directly. (a) Kinetics of the SNA assembly with the direct addition of varied concentrations of linker strand. [SNA-1] = [SNA-2] = 4 nM. (b) The curve of the linker strand concentration dependent value of τ.

It is clear that the linkage between SNA-1 and SNA-2 will accelerate with increasing linker strand concentration (lines

DOI: 10.1021/jacs.5b07453
J. Am. Chem. Soc. 2015, 137, 14107−14113

from 0 to 137.4 nM in Figure 3a). However, we notice the reaction rate becomes slower at higher concentrations of linker L (lines from 137.4 to 392.3 nM in Figure 3a). This is because the excess addition of linker L will seal the active strands on the surface of SNAs. Detailed explanations can be found in Figure S6 (SI).

Integrated System. In contrast to the direct-linker-addition method, in which the reaction rate of the SNA conjugates' assembly is a simple function of the amount of linker strand, the integrated system can be regulated using multiple parameters, including the amount of m-F, substrate S, catassembler strand C, and the length of the toeholds, which enable the assembly of SNA conjugates to be controlled over a large rate span.

We first examine the concentration dependence of S on the reaction of the SNA assembly. Considering that L is initially prehybridized in S, the release of L should rely on the concentration of S. Fixing the mole ratio of S to m-F at 1/10 and the concentration of C at 7 nM, we observed a decrease of τ in the Avrami equation from 20.1 to 9.5 h with an increase in concentration of S from 137.4 to 392.3 nM, an indicator of remarkable acceleration to the SNA assembly (Figure 4). In addition, the influence of the m-F concentration-dependent reaction rate of the SNA assembly was shown in Figure S7 (SI).

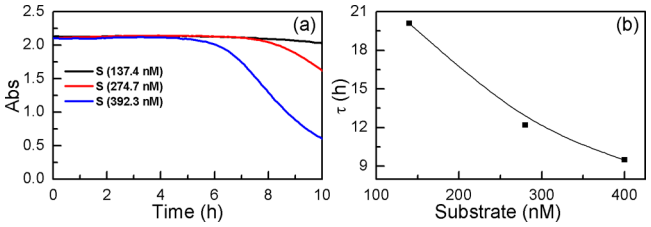

Figure 4. Influence of substrate on the reaction of the SNA assembly. (a) Kinetics of the SNA assembly with different concentrations of substrate. The toehold strategy for catassembler and protector was n/m = 5/5. [catassembler] = 7 nM, [substrate]/[m-F] = 1/10, [SNA-1] = [SNA-2] = 4 nM. (b) The curve of substrate concentration dependent value of τ.

Second, we examine the influence of toehold lengths on the SNA assembly. In the TMSDR, the light-blue domain (domain $\overline{\gamma^n}$, called toehold) in P of S is a necessary sequence for achieving a fast-forward branch-migration reaction to displace L by C, as illustrated in Figure S2 (SI), while the yellow domain (domain $\overline{\beta^m}$) exerts an inverse action against this forward procedure. Conceivably, the reaction responsible for the production of L should depend on the lengths of these two domains. On the basis of our experiences and other research,[15,18,52] a long light-blue toehold and/or short yellow domain are beneficial to the release of L because of two effects: the enhanced forward branch migration arising from the stronger binding strength of long light-blue toehold to its complement and the weakened inverse effect from the weaker binding of the short yellow domain with its counterpart. The SNA assembly is accelerated as expected, as a longer light-blue toehold is adopted while the yellow domain remains unchanged at a constant length of four bases (see lines n/m = 6/4 and 5/4, and lines n/m = 5/5 and 6/5 in Figure 5). However, in the cases of the yellow domain with a shortened sequence, the assembly of SNA is retarded rather than accelerated, as observed in the systems (domain γ^n = five or six bases) with

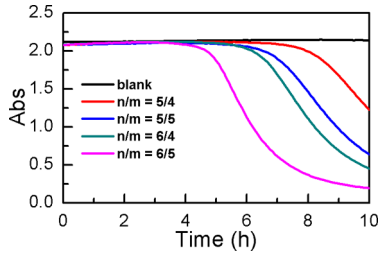

Figure 5. Influence of toehold lengths on the SNA assembly. The UV−vis kinetic curves show the reaction discrimination in different toehold strategies. [catassembler] = 7 nM, [substrate] = 392.3 nM, [m-F] = 3.92 μM, [SNA-1] = [SNA-2] = 4 nM.

four bases for the yellow domain compared with five bases (Figure 5). This nontrivial phenomenon is ascribed to the mutated base in the mismatched fuel strand. As shown in Figures 1 and S4 (SI), during the reaction displacing C by m-F from the double-stranded duplex made of C and P, the mismatched base in domain β^m of m-F in the five-base yellow-toehold strategy is simply required to jump over the exposed noncomplementary base in P to perform a displacement action (Figure S4a, SI). In contrast, the m-F in the four-base yellow-toehold approach has to overcome a high energy barrier to displace the covered noncomplementary base by C, as illustrated in Figure S4b (SI), thus significantly slowing the displacement reaction and then subsequently influencing the assembly of SNA.

Third, we examine the influence of the amount of the strand catassembler C on the SNA assembly. A number of techniques have now been developed for detecting a known sequence of oligonucleotide that relates to a specific disease,[57,58] among which SNA assembly assisted by the target DNA is one of the competitive approaches due to its advantage of easy signal readout arising from the plasmonic behavior of the gold core.[40] Definitely, the approach for a low limit of detection to an oligonucleotide target is always pursued. In our present instance, the linker strand L did not generate an observable signal until a concentration ~40 nM (blue line in Figure 3a), mimicking the traditional direct-linker-addition approach. On the other hand, the newly established strategy allows the conversion of the detection of the target strand from linker strand to catassembler strand C (Figure 1). With the assistance of this transformation, an accelerated reaction for SNA assembly can be readily achieved with a substoichiometric amount of the target strand, which is essential for low detection sensitivity. As shown in Figure 6, by increasing C on the order of 0.44 × 2^n nM, a series of remarkable signal outputs was

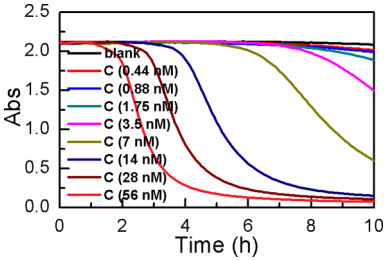

Figure 6. Kinetics of SNA assembly with different concentrations of catassembler. The toehold strategy for catassembler and protector was n/m = 5/5. [substrate] = 392.3 nM, [m-F] = 3.92 μM, [SNA-1] = [SNA-2] = 4 nM.

DOI: 10.1021/jacs.5b07453
J. Am. Chem. Soc. 2015, 137, 14107−14113

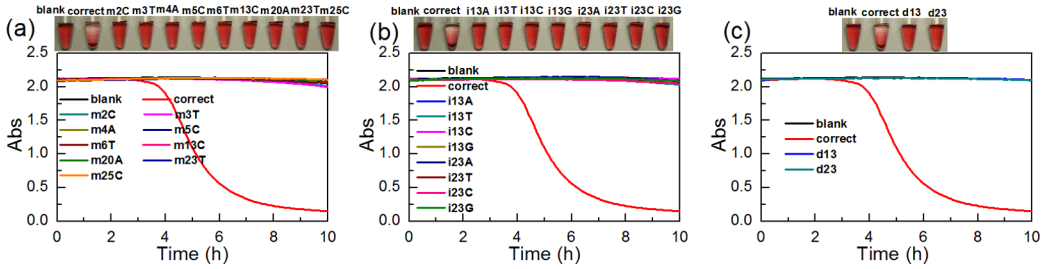

Figure 7. Kinetics of SNA assembly in which the correct and the spurious catassembler strands have a single-base mismatch (a), insertion (b), and deletion (c) at different positions. The inset panels show the corresponding color changes after 10 h. The labels "m", "i", and "d" represent mismatch, insertion, and deletion, respectively. The toehold strategy for catassembler and protector was n/m = 5/5. [catassembler] = 14 nM, [substrate] = 392.3 nM, [m-F] = 3.92 μM, [SNA-1] = [SNA-2] = 4 nM.

observed over a large concentration span. In particular, a distinguishable signal is achieved at 0.44 nM of C, constituting a ∼100-fold improvement relative to the direct-linker-addition approach.

In the integrated system, the linker strand binds to the protector strand initially in the double-stranded complex, substrate S. The addition of the catassembler strand will catalyze the upstream circuit and result in the gradual release of linker L. Compared with the direct-linker-addition systems, in which the linker strand is added in the initial setup, this strategy suffers from a relatively long duration time for the system to release the linker strands. Therefore, the gradually released linker strand can effectively link SNA-1 and SNA-2 together, and the active strands on the SNA surface will not be sealed under high linker concentration in the integrated system. The reaction rate increased upon increasing the concentration of substrate and catassembler strand.

An Application of the Integrated System for Single Nucleotide Polymorphism Discrimination. Developing sophisticated ways to discriminate single-base changes along an oligonucleotide sequence is highly desirable, since genetic single nucleotide polymorphisms in human DNA with one or more nucleotide changes, such as single-base mismatch, insertion, and deletion, are essential for the diagnosis of genetic diseases.[57,59−65]

As shown in Figures 1 and S2 (SI), the upstream catalytic circuit consists of multiple reactions. While a comprehensive reaction that governs the assembly processes of SNA conjugates can be systemically optimized, the approach also allows the regulation of each of the involved reactions individually for some specific purposes. With the help of theoretical analysis, we have optimized the toehold lengths to endow the integrated system with the capability to examine a single-base difference on a sequence of oligonucleotides. The five-step model for describing the toehold exchange reaction, developed in section S3 of the SI, presents the discrimination index D defined by $D = (k_{\{m,n\}}/k'_{\{m,n\}})$ (eq 31, SI). The detailed expression of D by $D = \{10/[1+(1/(6 \times 10^{6-n} + 10^{m-n}))]\}$ (eq 33, SI) suggests that a short length (n) of the toehold domain $\overline{\gamma^n}$ and longer length (m) of toehold $\overline{\beta^m}$ are beneficial to maximize discrimination. Considering that a very short toehold $\overline{\gamma^n}$ and long toehold $\overline{\beta^m}$ may potentially result in a retarded toehold-exchange reaction, we chose equal lengths for both toeholds of five bases in this strategy, i.e., $n = m = 5$. Interestingly, negligible changes were observed in both the UV−vis absorbance and color on a time scale of ∼10 h for the systems with the spurious targets' own single-base mismatch at different positions (Figure 7a), insertion (Figure 7b), and deletion (Figure 7c) in either the invading toehold region or the branch migration region, whereas the system with a correct target completed the reaction in ∼6 h (Figure 7a). The upper panels show that the cuvette in the system with the correct target is transparent after 6 h, owing to the sediment of aggregated SNAs. On the other hand, all of the samples from the spurious targets remain red, similar to the original states, which shows an all-or-none behavior, i.e., an obvious signal output when a correct target exists, in contrast to zero signal output in the presence of spurious targets.

CONCLUSIONS

In this present work, a strategy of integrating a strand-displacement-based DNA circuit with SNA conjugate assembly was established. This strategy provided a robust and reliable way of assembling SNAs in a programmable and algorithmic fashion. In our current methodology, the toehold-mediated strand-displacement catalytic circuit with SNA assembly is integrated by using two subsystems: the first subsystem serves as the upstream circuit to release a single DNA strand (linker L), and the second subsystem assembles the SNA conjugates triggered by the linker strand. The results can be easily monitored by UV−vis spectroscopy or by naked eye observations; that is, the DNA circuitry and nanoparticle aggregation are two sequential steps. These two steps can be combined into one test tube or separated from each other. The reactions driving the DNA circuits were independent of those of the SNA assembly, thus allowing the arbitrary choice of each quantity to make the DNA circuit operate at optimal states. Given that nanoparticle aggregation is only triggered by the linker strand released from the upstream circuit, we can manufacture different types of SNA conjugates with diverse external DNA shells on the basis of only one type of oligonucleotide-modified AuNPs to meet the large demand of diverse applications, therefore avoiding time-consuming and laborious procedures to functionalize diverse types of oligonucleotides on the surface of AuNPs.[51] Moreover, the DNA circuitry operates in free solution for homogeneous solutions. There are no steric hindrance problems that commonly associated with solid surface (such as nanoparticle surfaces),[66] facilitating the system with larger particles, such as microparticles and anisotropic particles. Since the two subsystems can be operated independently, the DNA circuit could conceivably be implemented a priori without the participation of SNAs. It could then transfer into the SNA solution for the assembly reaction, which will enable the two subsystems to be regulated under their own optimal conditions. Furthermore, linker strands are released from the DNA

DOI: 10.1021/jacs.5b07453
J. Am. Chem. Soc. 2015, 137, 14107−14113

circuitry gradually through toehold-mediated strand-displacement reaction in this strategy, rather than by adding the linker strand directly in the initial states, similar to the "direct-linker-addition strategy." This methodology ensures that the active oligomers on the surface of AuNPs will not be sealed and will not lose their activity in the initial setup. In summary, this new approach possesses several advantages over the previous methodology using the direct-linker-addition[51] and our DNA-machine-driven strategies.[49,50]

This strategy has been successfully implemented in the discrimination of single-mismatched bases in a sequence of oligonucleotides, which exhibits an improved discriminating ability relative to the former strategy, further confirming the advantages of this new engineering integration system. Finally, this should constitute a very promising strategy for other inorganic nanoparticle systems with well-established coordination chemistries (e.g., Ag, Pt, CdSe, and CdS), and the use of inorganic, anisotropic building blocks in our system may produce more attractive DNA−inorganic hybridization systems.

■ ASSOCIATED CONTENT

Supporting Information

The Supporting Information is available free of charge on the ACS Publications website at DOI: 10.1021/jacs.5b07453.

Experimental methods in detail, additional experimental results and supporting figures, analyses of DNA toehold exchange model, and DNA sequences (PDF)

■ AUTHOR INFORMATION

Corresponding Authors

*xiaosy@ustc.edu.cn
*hjliang@ustc.edu.cn

Author Contributions

H.L. and D.Y. conceived the project and designed the experiments. D.Y., T.S., X.S., and F.H. executed the experiments. S.X. designed and performed computational analyses. D.Y., S.X., and H.L. analyzed the results and wrote the manuscript. D.Y. and T.S. contributed equally to this work.

Notes

The authors declare no competing financial interest.

■ ACKNOWLEDGMENTS

We would like to thank the National Natural Science Foundation of China (Nos. 91427304, 21434007, 21574122, 51573175, 91127046, 21404097, and 21404098), the National Basic Research Program of China (No. 2012CB821500), and the Open Research Fund of State Key Laboratory of Polymer Physics and Chemistry (Changchun Institute of Applied Chemistry, Chinese Academy of Sciences) for their financial support.

■ REFERENCES

(1) Yurke, B.; Turberfield, A. J.; Mills, A. P., Jr.; Simmel, F. C.; Neumann, J. L. *Nature* **2000**, *406*, 605.
(2) Zhang, D. Y.; Seelig, G. *Nat. Chem.* **2011**, *3*, 103.
(3) Wang, F.; Lu, C.-H.; Willner, I. *Chem. Rev.* **2014**, *114*, 2881.
(4) Yan, H.; Park, S. H.; Finkelstein, G.; Reif, J. H.; LaBean, T. H. *Science* **2003**, *301*, 1882.
(5) Yan, H.; LaBean, T. H.; Feng, L.; Reif, J. H. *Proc. Natl. Acad. Sci. U. S. A.* **2003**, *100*, 8103.
(6) Tian, Y.; Mao, C. *J. Am. Chem. Soc.* **2004**, *126*, 11410.
(7) Yin, P.; Yan, H.; Daniell, X. G.; Turberfield, A. J.; Reif, J. H. *Angew. Chem., Int. Ed.* **2004**, *43*, 4906.
(8) Sherman, W. B.; Seeman, N. C. *Nano Lett.* **2004**, *4*, 1203.
(9) Tian, Y.; He, Y.; Chen, Y.; Yin, P.; Mao, C. *Angew. Chem., Int. Ed.* **2005**, *44*, 4355.
(10) Chen, X.; Briggs, N.; McLain, J. R.; Ellington, A. D. *Proc. Natl. Acad. Sci. U. S. A.* **2013**, *110*, 5386.
(11) Li, B.; Jiang, Y.; Chen, X.; Ellington, A. D. *J. Am. Chem. Soc.* **2012**, *134*, 13918.
(12) Lund, K.; Manzo, A. J.; Dabby, N.; Michelotti, N.; Johnson-Buck, A.; Nangreave, J.; Taylor, S.; Pei, R.; Stojanovic, M. N.; Walter, N. G.; Winfree, E.; Yan, H. *Nature* **2010**, *465*, 206.
(13) Venkataraman, S.; Dirks, R. M.; Rothemund, P. W. K.; Winfree, E.; Pierce, N. A. *Nat. Nanotechnol.* **2007**, *2*, 490.
(14) Zhang, D. Y.; Turberfield, A. J.; Yurke, B.; Winfree, E. *Science* **2007**, *318*, 1121.
(15) Zhang, D. Y.; Winfree, E. *J. Am. Chem. Soc.* **2009**, *131*, 17303.
(16) Zhang, D. Y.; Hariadi, R. F.; Choi, H. M. T.; Winfree, E. *Nat. Commun.* **2013**, *4*, 1965.
(17) Franco, E.; Friedrichs, E.; Kim, J.; Jungmann, R.; Murray, R.; Winfree, E.; Simmel, F. C. *Proc. Natl. Acad. Sci. U. S. A.* **2011**, *108*, E784.
(18) Qian, L.; Winfree, E. *Science* **2011**, *332*, 1196.
(19) Seelig, G.; Soloveichik, D.; Zhang, D. Y.; Winfree, E. *Science* **2006**, *314*, 1585.
(20) Qian, L.; Winfree, E.; Bruck, J. *Nature* **2011**, *475*, 368.
(21) Mirkin, C. A.; Letsinger, R. L.; Mucic, R. C.; Storhoff, J. J. *Nature* **1996**, *382*, 607.
(22) Alivisatos, A. P.; Johnsson, K. P.; Peng, X.; Wilson, T. E.; Loweth, C. J.; Bruchez, M. P.; Schultz, P. G. *Nature* **1996**, *382*, 609.
(23) Cutler, J. I.; Auyeung, E.; Mirkin, C. A. *J. Am. Chem. Soc.* **2012**, *134*, 1376.
(24) Claridge, S. A.; Liang, H. W.; Basu, S. R.; Fréchet, J. M. J.; Alivisatos, A. P. *Nano Lett.* **2008**, *8*, 1202.
(25) Yao, G.; Li, J.; Chao, J.; Pei, H.; Liu, H.; Zhao, Y.; Shi, J.; Huang, Q.; Wang, L.; Huang, W.; Fan, C. *Angew. Chem., Int. Ed.* **2015**, *54*, 2966.
(26) Auyeung, E.; Morris, W.; Mondloch, J. E.; Hupp, J. T.; Farha, O. K.; Mirkin, C. A. *J. Am. Chem. Soc.* **2015**, *137*, 1658.
(27) Chi, C.; Vargas-Lara, F.; Tkachenko, A. V.; Starr, F. W.; Gang, O. *ACS Nano* **2012**, *6*, 6793.
(28) Song, S.; Liang, Z.; Zhang, J.; Wang, L.; Li, G.; Fan, C. *Angew. Chem., Int. Ed.* **2009**, *48*, 8670.
(29) Nykypanchuk, D.; Maye, M. M.; van der Lelie, D.; Gang, O. *Nature* **2008**, *451*, 549.
(30) Auyeung, E.; Li, T. I. N. G.; Senesi, A. J.; Schmucker, A. L.; Pals, B. C.; de la Cruz, M. O.; Mirkin, C. A. *Nature* **2014**, *505*, 73.
(31) Storhoff, J. J.; Lucas, A. D.; Garimella, V.; Bao, Y. P.; Muller, U. R. *Nat. Biotechnol.* **2004**, *22*, 883.
(32) Wu, P.; Hwang, K.; Lan, T.; Lu, Y. *J. Am. Chem. Soc.* **2013**, *135*, 5254.
(33) Yan, X.; Blacklock, J.; Li, J.; Möhwald, H. *ACS Nano* **2012**, *6*, 111.
(34) Muroski, M. E.; Carnevale, K. J. F.; Riskowski, R. A.; Strouse, G. F. *ACS Nano* **2015**, *9*, 124.
(35) Rosi, N. L.; Giljohann, D. A.; Thaxton, C. S.; Lytton-Jean, A. K. R.; Han, M. S.; Mirkin, C. A. *Science* **2006**, *312*, 1027.
(36) Chou, L. Y. T.; Zagorovsky, K.; Chan, W. C. W. *Nat. Nanotechnol.* **2014**, *9*, 148.
(37) Douglas, S. M.; Bachelet, I.; Church, G. M. *Science* **2012**, *335*, 831.
(38) Giljohann, D. A.; Seferos, D. S.; Daniel, W. L.; Massich, M. D.; Patel, P. C.; Mirkin, C. A. *Angew. Chem., Int. Ed.* **2010**, *49*, 3280.
(39) Liu, J.; Lu, Y. *J. Am. Chem. Soc.* **2003**, *125*, 6642.
(40) Guo, L.; Xu, Y.; Ferhan, A. R.; Chen, G.; Kim, D.-H. *J. Am. Chem. Soc.* **2013**, *135*, 12338.
(41) Bai, X.; Shao, C.; Han, X.; Li, Y.; Guan, Y.; Deng, Z. *Biosens. Bioelectron.* **2010**, *25*, 1984.

DOI: 10.1021/jacs.5b07453
J. Am. Chem. Soc. 2015, 137, 14107−14113

(42) Baeissa, A.; Dave, N.; Smith, B. D.; Liu, J. *ACS Appl. Mater. Interfaces* **2010**, *2*, 3594.
(43) Smith, B. D.; Liu, J. *J. Am. Chem. Soc.* **2010**, *132*, 6300.
(44) Tan, L. H.; Xing, H.; Chen, H.; Lu, Y. *J. Am. Chem. Soc.* **2013**, *135*, 17675.
(45) Elbaz, J.; Cecconello, A.; Fan, Z.; Govorov, A. O.; Willner, I. *Nat. Commun.* **2013**, *4*, 2000.
(46) Zhao, Z.; Chen, C.; Dong, Y.; Yang, Z.; Fan, Q.-H.; Liu, D. *Angew. Chem., Int. Ed.* **2014**, *53*, 13468.
(47) Park, S.-J.; Taton, T. A.; Mirkin, C. A. *Science* **2002**, *295*, 1503.
(48) Thacker, V. V.; Herrmann, L. O.; Sigle, D. O.; Zhang, T.; Liedl, T.; Baumberg, J. J.; Keyser, U. F. *Nat. Commun.* **2014**, *5*, 3448.
(49) Song, T.; Liang, H. *J. Am. Chem. Soc.* **2012**, *134*, 10803.
(50) Song, T.; Xiao, S.; Yao, D.; Huang, F.; Hu, M.; Liang, H. *Adv. Mater.* **2014**, *26*, 6181.
(51) Jin, R.; Wu, G.; Li, Z.; Mirkin, C. A.; Schatz, G. C. *J. Am. Chem. Soc.* **2003**, *125*, 1643.
(52) Yurke, B.; Mills, A., Jr. *Genet. Program. Evolvable Mach.* **2003**, *4*, 111.
(53) Zhang, D. Y.; Winfree, E. *Nucleic Acids Res.* **2010**, *38*, 4182.
(54) Jiang, Y. S.; Bhadra, S.; Li, B.; Ellington, A. D. *Angew. Chem., Int. Ed.* **2014**, *53*, 1845.
(55) Machinek, R. R. F.; Ouldridge, T. E.; Haley, N. E. C.; Bath, J.; Turberfield, A. J. *Nat. Commun.* **2014**, *5*, 5324.
(56) Genot, A. J.; Zhang, D. Y.; Bath, J.; Turberfield, A. J. *J. Am. Chem. Soc.* **2011**, *133*, 2177.
(57) Patolsky, F.; Weizmann, Y.; Katz, E.; Willner, I. *Angew. Chem., Int. Ed.* **2003**, *42*, 2372.
(58) MacAskill, A.; Crawford, D.; Graham, D.; Faulds, K. *Anal. Chem.* **2009**, *81*, 8134.
(59) Subramanian, H. K. K.; Chakraborty, B.; Sha, R.; Seeman, N. C. *Nano Lett.* **2011**, *11*, 910.
(60) Xu, H.; Deng, W.; Huang, F.; Xiao, S.; Liu, G.; Liang, H. *Chem. Commun.* **2014**, *50*, 14171.
(61) Li, H.; Xiao, S.; Yao, D.; Lam, M. H.-W.; Liang, H. *Chem. Commun.* **2015**, *51*, 4670.
(62) Khodakov, D. A.; Khodakova, A. S.; Huang, D. M.; Linacre, A.; Ellis, A. V. *Sci. Rep.* **2015**, *5*, 8721.
(63) Chen, S. X.; Zhang, D. Y.; Seelig, G. *Nat. Chem.* **2013**, *5*, 782.
(64) Zhang, D. Y.; Chen, S. X.; Yin, P. *Nat. Chem.* **2012**, *4*, 208.
(65) Wu, Y.; Zhang, D. Y.; Yin, P.; Vollmer, F. *Small* **2014**, *10*, 2067.
(66) Yao, D.; Wang, B.; Xiao, S.; Song, T.; Huang, F.; Liang, H. *Langmuir* **2015**, *31*, 7055.

DOI: 10.1021/jacs.5b07453
J. Am. Chem. Soc. 2015, 137, 14107−14113